# Structure and Properties of Supramolecular Polymers Generated from Heterocomplementary Monomers Linked through Sextuple Hydrogen-Bonding Arrays

**E. Kolomiets,[†] E. Buhler,[‡] S. J. Candau,*[,†] and J.-M. Lehn*[,†]**

*I.S.I.S., Laboratoire de Chimie Supramoléculaire, ESA CNRS 7006, Université Louis Pasteur, 8 allée Gaspard Monge, 67083 Strasbourg Cedex, France, and Laboratoire de Spectrométrie Physique, UMR CNRS 5588, Université Joseph Fourier de Grenoble, BP87, 38402 St. Martin d'Hères, France*

*Received November 4, 2005*

ABSTRACT: The synthesis of homoditopic heterocomplementary monomers forming sextuple hydrogen-bond-mediated self-assemblies in apolar solvents is described. The nanostructures of the fibrillar aggregates formed in decane solutions of such monomers were investigated by small-angle neutron scattering. The fibers were found to be rigid, with an average length that increases upon increasing concentration and/or decreasing temperature. The cross section and the mass per unit length of the fibrillar aggregates are constant in the explored concentration range spanning both the dilute and semidilute regimes. These parameters are also insensitive to a temperature change. From the values of the cross section and of the mass per unit length, it can be inferred that the fibers contain on the average several monomolecular wires.

## 1. Introduction

Supramolecular polymers[1] are an increasingly important class of polymers, where designed intermolecular interactions allow a specific tailoring of polymer properties. In contrast to covalently linked polymers, new types of features of both structural ordering and dynamic nature due to the reversibility of the noncovalent connections have been achieved, opening the way in particular to a biologically inspired structuring of polymers on the nano- and microscale.[2]

The concept of supramolecular polymer chemistry has been developed by manipulating the intermolecular forces (such as hydrogen bonds,[3] ionic forces,[4] metal complexes,[5] $\pi-\pi$ stacking,[6] and steric interactions[7]) that lead to the formation of supramolecular structures.

Directed hydrogen bonds[3] have been shown particularly effective in that they allow the tuning of binding constants from the $M^{-1}$ domain up to $10^7$ $M^{-1}$, as well as the selective, recognition-directed, association between molecular monomers bearing complementary headgroups, through the use of specific hydrogen-bond matching pairs. Additionally, the ability to select specific intermolecular bonding patterns within several possibilities is specially versatile for hydrogen-bonding arrays. The reversibility of the interaction confers constitutional dynamic features that characterize supramolecular dynamers, dynamic polymers of supramolecular nature. These properties together with the relative ease of synthetic implementation have speeded up the application of hydrogen bonds as directing forces leading to supramolecular polymers.

The formation of reversible polymers resulting from the association of monomeric components through single to quadruple hydrogen-bonding arrays has been reported.[8−23] Recently, supramolecular polymers were derived from the association of two homoditopic heterocomplementary monomers through sextuple hydrogen-bonding arrays.[10] The strong affinity of the DAD-DAD (D = donor, A = acceptor) hydrogen-bonding sites for double-faced cyanuric acid-type wedges drives the supramolecular polymeric assembly in organic solvents of low polarity.

Variable temperature $^1$H NMR experiments performed in tetrachloroethane give evidence of a partial rupture of the hydrogen bonds that hold the polymeric assemblies together. However, the molecular weight of the polymer formed in chlorinated organic solvents is rather limited, as the solutions at concentrations up to $C = 10$ mM remain fluid.

In apolar solvents, like toluene, the formation of highly viscoelastic solutions was observed at concentrations as low as 2 mM, thus indicating well-ordered polymeric assemblies. Electron microscopy studies revealed the formation of rigid fibers. However, the systems investigated were found to be unstable over time.

The present study had two aims. The first one was to derive from the previously investigated entities based on sextuple hydrogen-bonding arrays, a system that would remain stable in time and behave reversibly under mechanical and temperature cycling. This was achieved by using solutions in decane of the supramolecular polymer $[AA9:BB]_n$ shown in Figure 1, involving a component AA9 bearing decanoyl side chains.

The second aim of the study was to establish the structure of the polymeric aggregates through small-angle neutron scattering (SANS). The results obtained show that the homoditopic monomers self-assemble into long rigid fibrillar aggregates whose length increases upon increasing concentration and/or decreasing temperature.

## 2. Experimental Section

**Materials.** THF was distilled over sodium/benzophenone. Absolute DMF (dried over molecular sieves, $H_2O < 0.005\%$) was purchased from Fluka. Triethylamine (Lancaster, 99%) was used as received. 2,6-Diaminopyridine (Aldrich, 98%) was purified by recrystallization from hot chloroform after filtration with charcoal. All other commercially available products were used without further purification. Flash column chromatography was performed using silica gel (Geduran, SI 60, 40−63 $\mu$m, Merck). 400 MHz $^1$H NMR spectra and 100 MHz $^{13}$C NMR spectra were recorded on a Bruker

[†] Université Louis Pasteur.
[‡] Université Joseph Fourier de Grenoble.

10.1021/ma0523522 CCC: $33.50 
Published on Web 01/07/2006

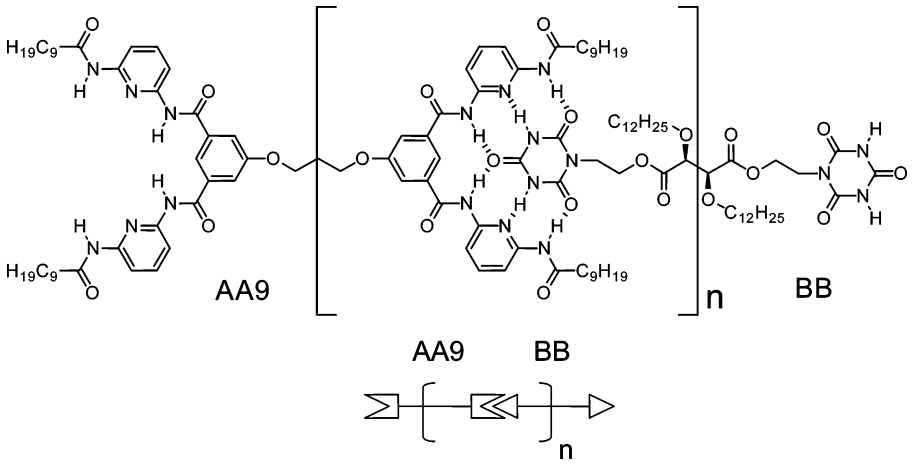


**Figure 1.** Linear supramolecular polymer [AA9:BB]$_n$ formed by H-bond-mediated molecular recognition between heterocomplementary binding sites of homoditopic bisreceptor AA9 and homoditopic biswedge BB.

Avance 400 spectrometer, and 200 MHz $^1$H NMR spectra and 50 MHz $^{13}$C NMR spectra were recorded on a Bruker SY 200 spectrometer. The solvent signal was used as an internal reference for both $^1$H and $^{13}$C NMR spectra. FAB-mass spectrometric measurements were performed by the Service de Spectrométrie de Masse, Institut de Chimie, Université Louis Pasteur. Electrospray studies were performed on a Bruker Micro TOF mass spectrometer. Melting points (mp) were recorded on a Büchi Melting Point B-540 apparatus and are uncorrected. Elemental analyses were performed by the Service de Microanalyse, Institut de Chimie, Université Louis Pasteur.

**Synthesis.** Products **6** and **7** are described in ref 10. 1-Nitrobiuret (**10**) was prepared following procedures in ref 24. L-*O*,*O*-Didodecyltartaric acid is described in ref 25.

**Decanoic Acid (6-Aminopyridin-2-yl)amide**, **5.** 2,6-Diaminopyridine, **4** (13.34 g, 122.2 mmol, 100 mol %), and triethylamine (12.37 g, 122.2 mmol, 100 mol %) were dissolved in dry THF (700 mL), and the solution was cooled to 0 °C in an ice bath. A solution of decanoyl chloride (24.48 g, 128.3 mmol, 105 mol %) in dry THF (180 mL) was added dropwise over a period of 1.5 h, and the reaction was allowed to proceed at 0 °C for 3 h, before warming to room temperature (rt). Then reaction mixture was filtered, evaporated to dryness, and purified using flash chromatography ($SiO_2$; 10% EtOAc/$CH_2Cl_2$ → 20% EtOAc/$CH_2Cl_2$) to give **5** (24.86 g, 77%) as a gray solid; mp 54.3−55.7 °C. IR (thin film): $\tilde{\nu}$ = 3473, 3348, 3199, 2925, 2854, 1679, 1619, 1578, 1537, 1455, 1353, 1295, 1249, 1160, 792 cm$^{-1}$. $^1$H NMR (200 MHz, [D$_6$]DMSO): $\delta$ = 9.76 (br s, 1 H); 7.28 (sm, 2 H); 6.16 (dd, $^3J$ = 6.5 Hz, $^4J$ = 2.3 Hz, 1 H); 5.67 (br s, 2 H); 2.31 (t, $^3J$ = 7.3 Hz, 2 H); 1.54 (sm, 2 H); 1.27 (sm, 12 H); 0.84 (t, $^3J$ = 6.3 Hz, 3 H). $^{13}$C NMR (50 MHz, [D$_6$]DMSO): $\delta$ = 171.5; 158.3; 150.4; 138.6; 103.0; 100.8; 36.0; 31.2; 28.8; 28.7; 28.6; 28.5; 25.0; 22.0; 13.8. FAB-MS: *m*/*z* 264.2 ([M + H]$^+$, 100%). Anal. Calcd for $C_{15}H_{25}N_3O$ (263.39): C 68.40, H 9.57, N 15.95. Found: C 68.53, H 9.57, N 16.02.

**1,3-Bis(3,5-bis(6-decanoylaminopyridin-2-ylcarbamoyl)phenoxy)propane, 1.** Tetraacid **7**[10] (2.57 g, 6.4 mmol, 100 mol %) was suspended in $SOCl_2$ (60 mL). A drop of dry DMF was added, and the solution was heated to reflux. After 20 min the solid had entirely dissolved, and the solution was refluxed for a further 14 h. The excess $SOCl_2$ was distilled off, and the oily residue was kept under high vacuum for 50 min to afford the crude tetraacid chloride **7a**, which was used as such. **7a** was dissolved in THF (40 mL) and cannulated into a previously prepared solution of **5** (6.93 g, 26.3 mmol, 414 mol %) and triethylamine (3.71 mL, 26.7 mmol, 420 mol %) in THF (60 mL) at rt. The reaction was allowed to proceed for 18 h, after which time the reaction mixture was filtered, evaporated to dryness, and chromatographed ($SiO_2$; EtOAc/hexane 30:70). **1** (6.87 g, 78%) was obtained as a slightly yellow powder; mp 187.8−190.2 °C. $^1$H NMR (400 MHz, [D$_6$]DMSO): $\delta$ = 10.47 (s, 4 H); 10.07 (s, 4 H); 8.13 (s, 2 H); 7.82 (sm, 16 H); 4.37 (br t, $^3J$ = 6.4 Hz, 4 H); 2.38 (t, $^3J$ = 7.8 Hz, 8 H); 2.32 (br m, 2 H); 1.57 (m, 8 H); 1.23 (sm, 48 H); 0.84 (t, $^3J$ = 7.1 Hz, 12 H). $^{13}$C NMR (100 MHz, [D$_6$]DMSO): $\delta$ = 172.2; 164.9; 158.5; 150.6; 150.0; 140.0; 135.6; 119.8; 117.2; 110.4; 109.9; 64.9; 36.1; 31.3; 28.7; 25.0; 22.1; 13.9. FAB-MS: *m*/*z* 1385.6 ([M]$^+$, 100%). Anal. Calcd for $C_{79}H_{108}N_{12}O_{10}$ (1385.78): C 68.47, H 7.86, N 12.13. Found: C 68.14, H 7.96, N 11.76.

***N*-(2-Hydroxyethyl)phthalimide, 11.** Phthalic anhydride (71.8 g, 0.48 mol, 100 mol %) was added gradually, under agitation, to 2-aminoethanol, **8** (30.5 g, 0.50 mol, 104 mol %). On completion of this addition, the solution was heated to 100 °C for 30 min, and after cooling to rt, 200 mL of hot water was added. The product **11** precipitated as a white solid, which was filtered and dried. Yield 52.8 g (57%); mp 128.3−131.1 °C. $^1$H NMR (400 MHz, [D]chloroform): $\delta$ = 7.79 (m, 2 H); 7.68 (m, 2 H); 3.84 (m, 4 H). $^{13}$C NMR (100 MHz, [D]chloroform): $\delta$ = 168.9; 134.1; 132.0; 123.4; 60.8; 40.8. FAB-MS: *m*/*z* 192.0 ([M + H]$^+$, 100%). Anal. Calcd for $C_{10}H_9NO_3$ (191.18): C 62.82, H 4.74, N 7.33. Found: C 62.67, H 4.74, N 7.23.

**2-Phthalimidoethylbenzyl Ether, 12.** (5.0 g, 0.125 mol, 120 mol %) of sodium hydride (60% in oil) was suspended in 100 mL of dry DMF under an atmosphere of nitrogen. Then **11** (20.0 g, 0.104 mol, 100 mol %) was added at rt. After another 15 min benzyl bromide (13.6 mL, 0.115 mol, 110 mol %) was added dropwise under nitrogen. The reaction mixture was heated to 80 °C and refluxed for 2 h. The reaction was cooled and concentrated in vacuo, and the residue was partitioned between $CH_2Cl_2$ (250 mL) and $H_2O$ (100 mL). The organic extract was dried over $Na_2SO_4$ and concentrated in vacuo. The product **12** was recrystallized from diethyl ether/hexane to give 24.1 g (82%) of a beige solid; mp 71.9−72.0 °C. $^1$H NMR (400 MHz, [D]chloroform): $\delta$ = 7.87−7.82 (m, 2 H); 7.74−7.70 (m, 2 H); 7.28−7.20 (m, 5 H); 4.54 (s, 2 H); 3.94 (t, $^3J$ = 5.6 Hz, 2 H); 3.73 (t, $^3J$ = 5.6 Hz, 2 H). $^{13}$C NMR (100 MHz, [D]chloroform): $\delta$ = 168.1; 137.7; 133.7; 132.0; 128.1; 127.5; 123.1; 72.5; 66.6; 37.3. FAB-MS: *m*/*z* 282.3 ([M + H]$^+$, 100%). HRMS (FAB-MS): calcd for [$C_{17}H_{15}NO_3$ + H]: 282.1130; found: 282.1127. Anal. Calcd for $C_{17}H_{15}NO_3$ (281.31): C 72.58, H 5.37, N 4.98. Found: C 72.34, H 5.33, N 4.96.

**2-*O*-Benzylethanolamine, 13.** To **12** (22.13 g, 78.7 mmol, 100 mol %) in 109 mL of ethanol was added hydrazine monohydrate (18.51 g, 370 mmol, 470 mol %). The mixture was stirred at rt under argon for 14 h. The reaction was diluted with dichloromethane (200 mL) and filtered. The filtrate was concentrated in vacuo and extracted two times with 50 mL portions of 2 M aqueous HCl. The combined aqueous phases were washed with diethyl ether (2 × 50 mL), then were basified with sodium hydroxide anhydrous pellets, and finally extracted with dichloromethane. The organic extract was dried over $Na_2SO_4$ and concentrated in vacuo to give 8.1 g (68%) of the product **13** as a yellow liquid. $^1$H NMR (400

MHz, [D]chloroform): $\delta$ = 7.32−7.23 (m, 5 H); 4.50 (s, 2 H); 3.48 (t, $^3J$ = 5.0 Hz, 2 H); 2.86 (t, $^3J$ = 5.0 Hz, 2 H). $^{13}$C NMR (100 MHz, [D]chloroform): $\delta$ = 138.4; 128.4; 127.7; 73.0; 72.4; 41.9. FAB-MS: *m*/*z* 152.2 ([M + H]$^+$, 100%). HRMS (FAB-MS): calcd for [$C_9H_{13}NO$ + H]: 152.1075; found: 152.1076.

**1-(2-Benzyloxyethyl)biuret, 14.** To a solution of **13** (9.1 g, 60 mmol, 100 mol %) in 110 mL of water 1-nitrobiuret **10** (8.9 g, 60 mmol, 100 mol %) was added portionwise. The reaction was heated to reflux under nitrogen for 3.5 h and cooled in an ice bath, and the precipitated product was collected by vacuum filtration and washed with 200 mL of water. The product was dried, giving 10.7 g (75%) of the product **14** as a white solid; mp 135.1−136.3 °C. $^1$H NMR (400 MHz, [D]chloroform): $\delta$ = 9.10 (br s, 1 H); 7.36−7.29 (m, 5 H); 4.57 (s, 2 H); 3.64 (t, $^3J$ = 5.3 Hz, 2 H); 3.51 (t, $^3J$ = 5.2 Hz, 2 H). $^{13}$C NMR (100 MHz, [D$_6$]DMSO): $\delta$ = 155.5; 154.5; 138.3; 128.2; 127.5; 71.8; 68.6; 54.7. FAB-MS: *m*/*z* 238.3 ([M + H]$^+$, 100%). HRMS (FAB-MS): calcd for [$C_{11}H_{15}N_3O_3$ + H]: 238.1192; found: 238.1196. Anal. Calcd for $C_{11}H_{15}N_3O_3$ (237.26): C 55.69, H 6.37, N 17.71. Found: C 55.75, H 6.30, N 17.56.

***N*-(2-Benzyloxyethyl)isocyanuric Acid, 15.** Sodium metal (1.92 g, 83.5 mmol, 330 mol %) was dissolved in 66 mL of absolute ethanol under nitrogen. Then **14** (6.0 g, 25.3 mmol, 100 mol %) was added followed by 6.6 mL of diethyl carbonate (54.4 mmol, 215 mol %). The mixture was heated under nitrogen to reflux for 13 h. The reaction was cooled to rt, diluted with toluene (150 mL) and ethanol (120 mL), and concentrated in vacuo. The residue was diluted with water (90 mL), cooled in an ice bath, and acidified with 36% hydrochloric acid to a pH of 1.0. The precipitated product was collected by vacuum filtration, washed with 200 mL of water, and dried to give 5.7 g (85%) of the product **15** as a white solid; mp 193.5−195.3 °C. $^1$H NMR (400 MHz, [D$_6$]DMSO): $\delta$ = 11.44 (br s, 2 H); 7.35−7.27 (m, 5 H); 4.47 (s, 2 H); 3.88 (t, $^3J$ = 6.1 Hz, 2 H); 3.58 (t, $^3J$ = 6.1 Hz, 2 H). $^{13}$C NMR (100 MHz, [D$_6$]DMSO): $\delta$ = 149.9; 148.7; 138.4; 128.3; 127.5; 71.7; 66.2; 39.7. FAB-MS: *m*/*z* 264.3 ([M + H]$^+$, 72%). HRMS (FAB-MS): calcd for [$C_{12}H_{13}N_3O_4$ + H]: 264.0984; found: 264.0983. Anal. Calcd for $C_{12}H_{13}N_3O_4$ (263.25): C 54.75, H 4.98, N 15.96. Found: C 55.42, H 4.29, N 15.16.

***N*-(2-Hydroxyethyl)isocyanuric Acid, 16. 15** (0.76 g, 2.89 mmol, 100 mol %) was dissolved in 36 mL of absolute ethanol, and 10% palladium−charcoal (0.80 g) was added followed by the addition of cyclohexene (30 mL). The reaction was heated to reflux for 28 h. After cooling to rt, the mixture was filtered, washed with ethanol, and evaporated under reduced pressure to give 0.38 g (76%) of the product **16** as a beige solid; mp 209.8−215.7 °C. $^1$H NMR (400 MHz, [D$_4$]methanol): $\delta$ = 3.96 (t, $^3J$ = 5.8 Hz, 2 H); 3.73 (t, $^3J$ = 5.8 Hz, 2 H).$^{13}$C NMR (100 MHz, [D$_4$]methanol): $\delta$ = 152.0; 151.0; 60.0; 44.0. FAB-MS: *m*/*z* 174.2 ([M + H]$^+$, 70%). HRMS (FAB-MS): calcd for [$C_5H_7N_3O_4$ + H]: 174.0515; found: 174.0519. Anal. Calcd for $C_5H_7N_3O_4$ (173.13): C 34.69, H 4.08, N 24.27. Found: C 34.98, H 3.45, N 22.75.

**L-2,3-*O*,*O*-Didodecyltartaric Acid Bis[2-(2,4,6-trioxo[1,3,5]-triazinan-1-yl)ethyl] Ester, 2.** To a solution of L-*O*,*O*-didodecyltartaric acid[25] (0.50 g, 1.03 mmol, 100 mol %), **16** (0.53 g, 3.08 mmol, 300 mol %), andDMAP (0.15 g, 1.23 mmol, 120 mol %) in anhydrous pyridine (7.5 mL) at rt was added EDC (0.43 g, 2.26 mmol, 220 mol %). The reaction was allowed to proceed for 5 nights and then partitioned between diethyl ether (10 mL) and saturated aqueous $NaHSO_4$ (8 mL). The organic extract was dried over $Na_2SO_4$, evaporated onto $SiO_2$, and purified by column chromatography ($SiO_2$; 60% EtOAc/$CH_2Cl_2$) to give 0.48 g (58%) of the product **2** as a white solid; mp 139.7−145.8 °C. $^1$H NMR (400 MHz, [D]chloroform): $\delta$ = 9.35 (s, 4 H); 4.48−4.44 (m, 2 H); 4.32−4.30 (m, 2 H); 4.27 (s, 2 H); 4.23−4.15 (m, 4 H); 3.81 (dt, $^2J$ = 9.2 Hz, $^3J$ = 7.1 Hz, 2 H); 3.35 (dt, $^2J$ = 9.2 Hz, $^3J$ = 7.1 Hz, 2 H); 1.51 (m, 4 H); 1.23 (sm, 36 H); 0.88 (t, $^3J$ = 7.1 Hz, 6 H). $^{13}$C NMR (100 MHz, [D]chloroform): $\delta$ = 169.7; 149.6; 149.4; 79.5; 72.5; 61.7; 40.5; 32.0; 29.5; 26.1; 22.8; 14.2. FAB-MS: *m*/*z* 819.3 ([M + Na]$^+$, 80%). Anal. Calcd for $C_{38}H_{64}N_6O_{12}$ (796.95): C 57.27, H 8.09, N 10.55. Found: C 57.20, H 8.11, N 10.17.

**Viscosimetry.** Rheological studies on the supramolecular polymer systems [AA9:BB]$_n$ were performed with a controlled rate rheometer Brookfield DV-III+, using a cone−plate geometry (diameter 40 mm, 1°). The temperature was controlled using a water bath.

**Small-Angle Neutron Scattering (SANS).** SANS experiments were carried out on the spectrometer D11 in Laue Langevin Institut at Grenoble (ILL, France). The chosen incident wavelength $\lambda$ depends on the set of experiments, as follows. For a given wavelength, the range of the amplitude of the transfer wave vector $q$ was selected by changing the detector distance $D$. Four sets of sample-to-detector distances and wavelengths were chosen ($D$ = 1.75 m, $\lambda$ = 6 ± 0.5 Å; $D$ = 8 m, $\lambda$ = 6 ± 0.5 Å; $D$ = 28 m, $\lambda$ = 6 ± 0.5 Å; and $D$ = 34 m, $\lambda$ = 12.5 ± 1.0 Å) so that the following $q$ ranges were respectively available: $3.7 \times 10^{-2} \le q$ (Å$^{-1}$) $\le 2.1 \times 10^{-1}$, $8.1 \times 10^{-3} \le q$ (Å$^{-1}$) $\le 4.71 \times 10^{-2}$, $2 \times 10^{-3} \le q$ (Å$^{-1}$) $\le 1.41 \times 10^{-2}$, and $7.9 \times 10^{-4} \le q$ (Å$^{-1}$) $\le 6.64 \times 10^{-3}$. Measured intensities were calibrated to absolute values (cm$^{-1}$) using the normalization by the attenuated direct beam classical method. Standard procedures to correct the data for the transmission, detector efficiency, and backgrounds (solvent, empty cell, electronic, and neutronic background) were done. The scattered wave vector $q$ is defined by eq 1 where $\theta$ is the scattering angle.

$$q = \frac{4\pi}{\lambda}\sin\left(\frac{\theta}{2}\right) \tag{1}$$

The usual equation for absolute neutron scattering combines the intraparticle scattering $S_1(q) = V_{chain}\phi_{vol}P(q)$ form factor with the interparticule scattering $S_2(q)$ factor:

$$I(q)\ (\mathrm{cm}^{-1}) = \frac{1}{V}\frac{\mathrm{d}\sigma}{\mathrm{d}\Omega} = (\Delta\rho)^2(S_1(q) + S_2(q))$$

$$= (\Delta\rho)^2(V_{chain}\phi_{vol}P(q) + S_2(q)) \tag{2}$$

where $(\Delta\rho)^2 = (\rho_{monomer} - \rho_{solvent})^2$ is a contrast per unit volume between the polymer and the solvent and was determined from the known chemical composition. $\rho = \sum n_i b_i/(\sum n_i m_i \upsilon \times 1.66 \times 10^{-24})$ represents the scattering length per unit volume, $b_i$ is the neutron scattering length of the species $i$, $m_i$ is the mass of species $i$, and $\upsilon$ is the specific volume of the monomer or the solvent. $V_{chain} = N\upsilon m \times 1.66 \times 10^{-24}$ is the volume of the $N$ monomers (of mass $m$) in a chain, and $\phi_{vol}$ is the volume fraction of monomer. In the high $q$ range, the scattering is assumed to arise from isolated chains; i.e., $S_2(q) = 0$, and thus $I(q) \propto P(q)$.

## 3. Results

**A. Synthesis.** A convergent route for the synthesis of the cyanuric acid-based receptor **1** and the L-tartaric bis(cyanurate) **2** (Figures 2 and 3) was developed to facilitate access to preparative quantities of these materials.

The bis-receptor **1** with terminal decanoyl amides was obtained following the procedure described earlier[10] (Figure 2). *O*-Alkylation of dimethyl 5-hydroxyisophthalate **3** was accomplished with 1,3-dibromopropane to yield tetraester **6**. Ester **6** was subsequently hydrolyzed to its corresponding carboxylic acid **7** and converted to the acid chloride **7a**. Treatment of the acid chloride with separately prepared *N*-(6-aminopyridin-2-yl)-decanoamide (**5**) afforded receptor **1** in good yield. Monoamide **5** was obtained by statistical acylation of 2,6-diaminopyridine (**4**) with decanoyl chloride.

Synthesis of the L-tartaric bis(cyanurate) **2** (Figure 3) (termed biswedge **2**) was achieved by an EDC coupling of an alcohol **16** to previously described L-*O*,*O*-didodecyltartaric acid.[25] The alcohol **16** was obtained by protection of the amino group of 2-aminoethanol **8**, followed by hydroxyl group protection of the obtained *N*-(2-hydroxyethyl)phthalimide **11** to give benzyl ether **12**. Subsequent deprotection of the amino group of **12**

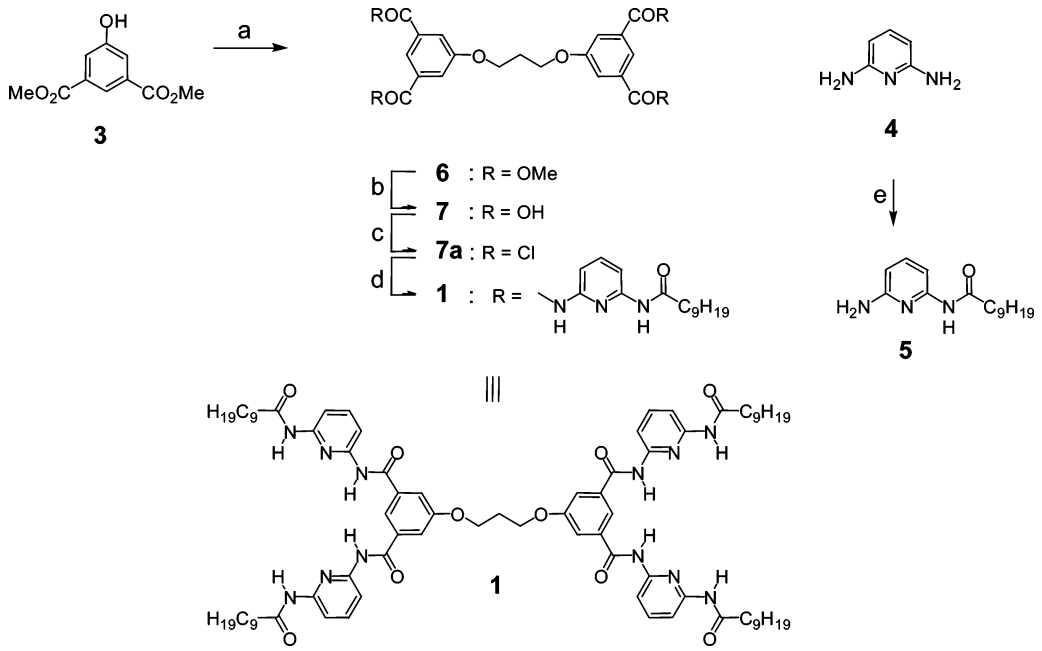


**Figure 2.** Synthesis of the homoditopic receptor **1**.

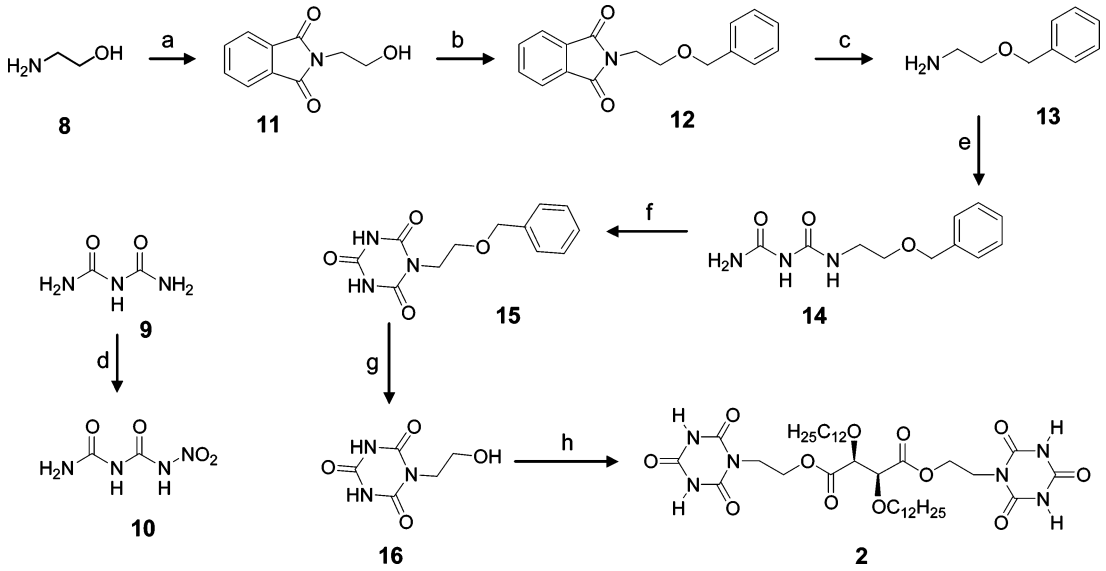


**Figure 3.** Synthesis of the ditopic substrate **2**.

yields 2-*O*-benzylethanolamide **13**, which was reacted with a previously prepared 1-nitrobiuret **10**[24] to give 1-(2-benzyloxyethyl)biuret **14**. Cyclization of **14**, followed by a hydrogenolysis of a benzyl group of the obtained *N*-(2-benzyloxyethyl)-isocyanuric acid **(15)**, yields the free alcohol **16**.

**B. Gel Formation.** Experimental observations reveal a strong correlation between the solubility of the monomers and the ability of the supramolecular polymers to form long polymeric assemblies. Thus, organogel formation by supramolecular systems $[AA9:BB]_n$ requires a very low solubility of both monomers (the bisreceptor and the biswedge) within a given solvent. Appreciable solubility of even one of the two molecular components results in the formation of limited chain length aggregates. In chlorinated organic solvents, like chloroform and tetrachloroethane, the bisreceptor AA9 and the biswedge BB dissolve readily, and the solutions of $[AA9:BB]_n$ system in these solvents remain highly fluid.

The supramolecular polymer formed from the bisreceptor AA9, which is soluble in toluene, and the biswedge BB, which is almost insoluble in this solvent, does not form viscous solutions. The above observations can be attributed to limited strength of the hydrogen-bonded associations which can also be expressed in terms of a scission energy (free energy penalty to create two new monomeric units exposed to solvent).

Bisreceptor AA9 and biswedge BB are almost insoluble in decane as individual compounds. In contrast, their mixtures in 1:1 stoichiometry dissolve readily in decane under heating to form transparent gels in decane at concentration $\geq 3$ mM of each component. The main driving force is the hydrogen-bond association-induced solubilization of the polar recognition functions in the apolar solvent. The apolar solvent environment in decane is expected to significantly increase the strength of the hydrogen-bonded associations, leading to higher order polymeric assemblies.

Solutions of $[AA9:BB]_n$ in decane are stable over time and thermal cycles and can be considered as systems at thermodynamic equilibrium. They lead to gel formation only above a concentration that can be identified as the crossover concentra-

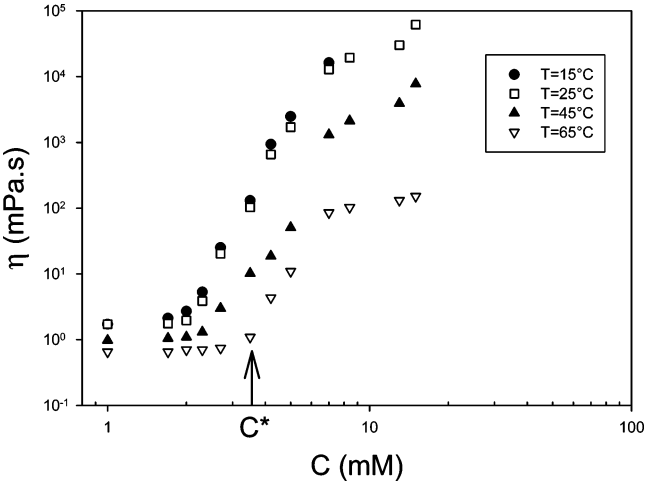


**Figure 4.** Viscosity at $\dot{\gamma} = 0.38\ s^{-1}$ of $[AA9:BB]_n$ in decane as a function of concentration at different temperatures. The arrow indicates the crossover concentration at $T = 65$ °C.

tion $C^*$ between dilute and semidilute regimes, which is the concentration beyond which the polymeric aggregates start to overlap each other. The crossover concentration $C^*$ and its temperature dependence were determined from viscosimetric measurements performed at the shear rate $\dot{\gamma} = 0.38\ s^{-1}$ (Figure 4).

The viscosity of dilute solutions of $[AA9:BB]_n$ in decane, which is close to that of the solvent in the dilute regime, increases markedly above the crossover concentration $C^*$. The apparent leveling off of the viscosity observed in the high concentration regime is due to the fact that the measurements have been performed at a fixed shear rate. The measured viscosity is smaller than the zero-shear viscosity because of the shear-thinning effect that occurs in these systems. The detailed rheological behavior will be reported in a forthcoming paper.

Figure 4 shows that $C^*$ increases with temperature, which can be explained in terms of the rupture of hydrogen bonds and subsequent shortening of the polymer chains.

Variable temperature $^1$H NMR experiments performed on the low-viscosity solutions of $[AA9:BB]_n$ in deuterated tetrachloroethane confirm the reversible rupture of hydrogen bonds under heating (Figure 5). When a 5 mM solution is heated from 25 to 100 °C, the $^1$H NMR spectra show a sharpening of the peaks and a shift of the amide proton signals (9.9 and 9.2 ppm) of the bisreceptor AA9 toward higher fields due to the partial rupture of the hydrogen bonds holding the polymeric assemblies together (Figure 5a). Upon subsequent cooling of the solution, the initial spectrum of the SPS is recovered, thus demonstrating the reversible rupture of hydrogen bonds (Figure 5b).

**C. Small-Angle Neutron Scattering (SANS) Studies.** Figure 6 shows the variations of the ratio $I/C$ of the scattered intensity over the concentration vs the scattering wave vector $q$ for $[AA9:BB]_n$ solutions in deuterated decane at various concentrations spanning both dilute and semidilute regimes at $T = 25$ °C.

The most interesting feature of Figure 6 concerns the intermediate $q$ range where all the scattering curves superimpose on each other, thus indicating that the self-assembled polymers have the same structure at the spatial scale corresponding to this $q$ range. Furthermore, the $q$ dependence of the scattered intensity can be described by a power law with an exponent close to $-1$, which suggests a rigid-rod structure.

The dip observed in the high $q$ range is the initial part of the oscillating term of the shape dependent form factor of the particle cross section.

In the low $q$ range, the shape of the scattering curves depends on whether the polymer concentration is close to or far from the crossover concentration $C^*$. At this temperature, $C^*$ is of the order of 2.2 mM in protonated decane. One cannot discard a small isotopic effect which would slightly affect this value of $C^*$.

Systems with $C \ll C^*$ or $C \gg C^*$ exhibit a Guinier regime with a plateau in the low $q$ range associated with the finite size of the scattering objects. In the vicinity of $C^*$ one observes a strong upturn of the scattered intensity in the low $q$ range and a crossover between a $q^{-1}$ and a $q^{-2}$ behavior upon decreasing $q$.

The effect of temperature is illustrated in Figure 7 which shows the scattering curves obtained for a 2 mM solution at 25 and 65 °C. The local structure is not modified by the temperature

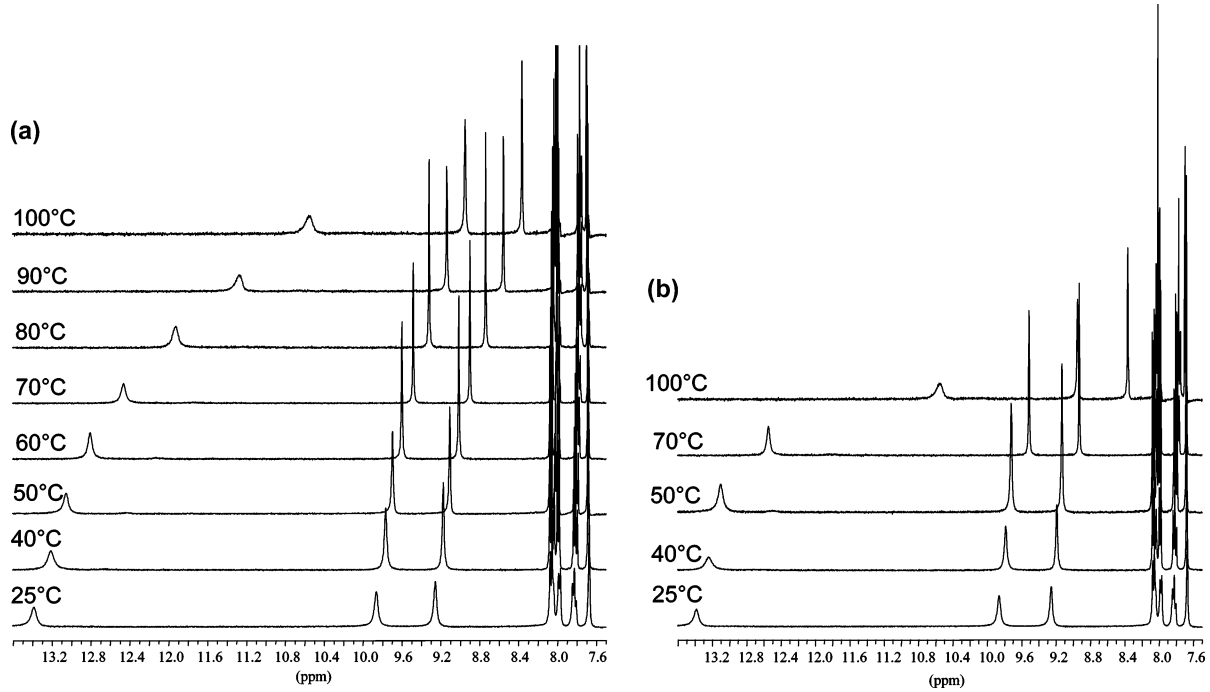


**Figure 5.** $^1$H NMR spectra at various temperatures for a 5 mM solution of $[AA9:BB]_n$ in $[D_2]$tetrachloroethane: (a) heating; (b) cooling.

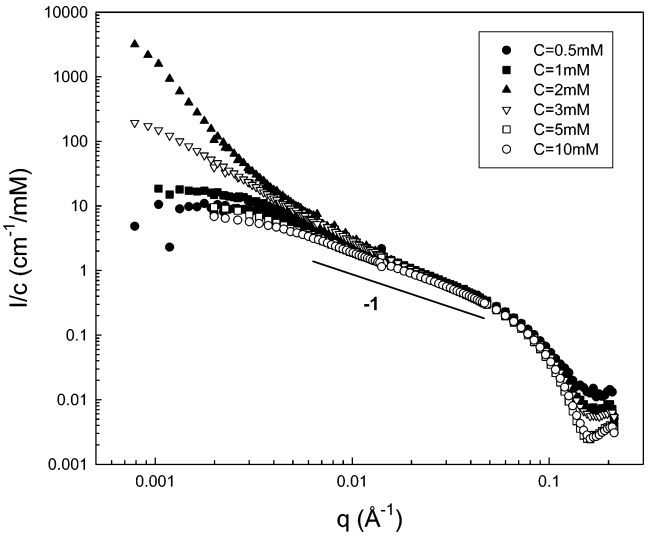


**Figure 6.** Variation of the ratio $I/C$ with $q$ obtained using SANS experiments for $[AA9:BB]_n$ solutions at various concentrations and at $T = 25$ °C.

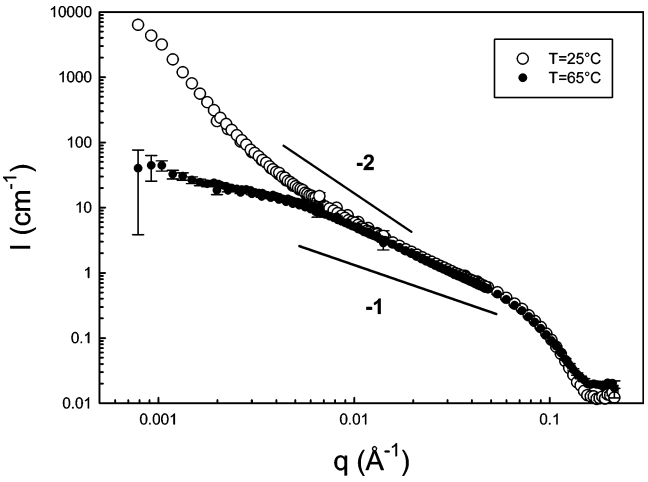


**Figure 7.** SANS scattering curve obtained for a 2 mM solution of $[AA9:BB]_n$ at 25 °C (○) and 65 °C (●).

change as shown by the superposition of the data in the intermediate and high $q$ ranges. The upturn of the scattering intensity in the low $q$ range occurring at 25 °C disappears at 65 °C, which indicates a breaking of the polymeric aggregates.

## 4. Discussion

**Correlation Length.** The low $q$ data have been fitted by the Ornstein−Zernicke law:

$$\frac{1}{I(q)} = \frac{1}{I(0)}(1 + q^2\xi^2) \tag{3}$$

where $\xi$ is the correlation length. Figure 8 shows the plot $I^{-1} = f(q^2)$ for two samples at concentration $C = 1$ mM and temperature $T = 25$ °C and $C = 2$ mM and $T = 65$ °C. From the best linear fit to the data one obtains values of the correlation length $\xi = 26$ and 20 nm, respectively.

In the dilute range the radius of gyration of the particle is given by $R_G = 3^{1/2}\xi$ and for rodlike particles with large aspect ratio, $R_G^2 = L^2/12$, where $L$ is the average contour length of the rod. For $C = 0.5$ and 1 mM at $T = 25$ °C we obtain $L = 103$ and 156 nm, respectively.

In Figure 9 are reported the variations of $\xi$ and of $I(q=0)$ as a function of concentration. For $C \ll C^*$ one observes a

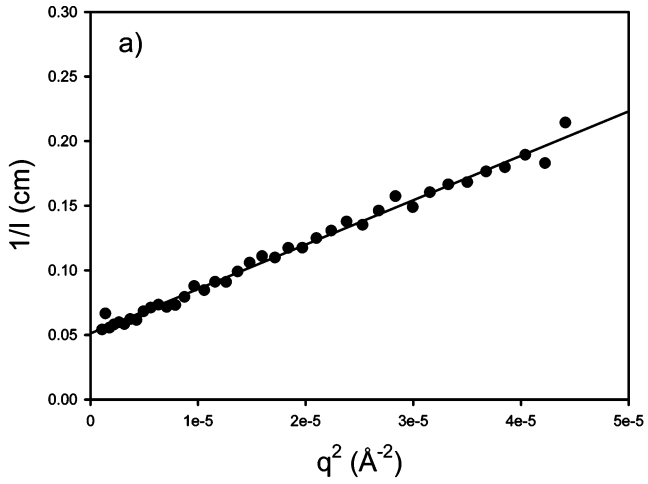


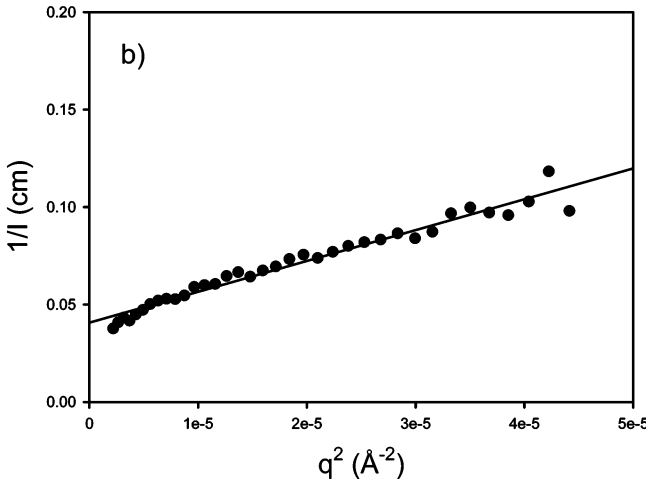


**Figure 8.** Variation of $1/I$ with $q^2$ for samples at concentration $C = 1$ mM and temperature $T = 25$ °C (a) and $C = 2$ mM and $T = 65$ °C (b).

moderate increase of $\xi$, in agreement with the model derived for equilibrium polymer that predict a $C^{1/2}$ dependence of the average length $L$ of the self-assembled polymer. For long rigid rods $L$ is proportional to $R_G$. The increase of $\xi$ (or $R_G$) observed over only two data point is in satisfactory agreement with the theoretical prediction. For $C \gg C^*$, the correlation length decreases, as in the regular polymer solutions because of the progressive interpenetration of the polymer aggregates that leads to $\xi \sim C^{-1/2}$. The most surprising observation concerns the behavior observed in the vicinity of $C^*$, where there is obviously formation of very large particles. At 2 mM concentration and 25 °C, which is very close to $C^*$, the low $q$ plateau is not reached, and one can obtain only a lower estimate of $\xi$. At high temperature, the particle breaks to reach a much smaller size. The behavior of $\xi$ is qualitatively corroborated by that of $I(q=0)$ (Figure 9b).

**Particle Conformation.** For $C \ll C^*$ or $C \gg C^*$, the scattering curves can be fitted satisfactorily by a rigid-rod model. Figure 10 shows the fits realized in the intermediate $q$ regimes for a 10 mM solution of $[AA9:BB]_n$, which is in the semidilute regime, by means of the des Cloizeaux law[26] derived for rigid-rod particles and valid for $qL_p > 2$, where $L_p$ is the persistence length.

$$P(q) = \frac{\pi}{qL} + \frac{2}{3q^2L_pL} \tag{4}$$

The high $q$ data can be fitted by a Guinier expression for the

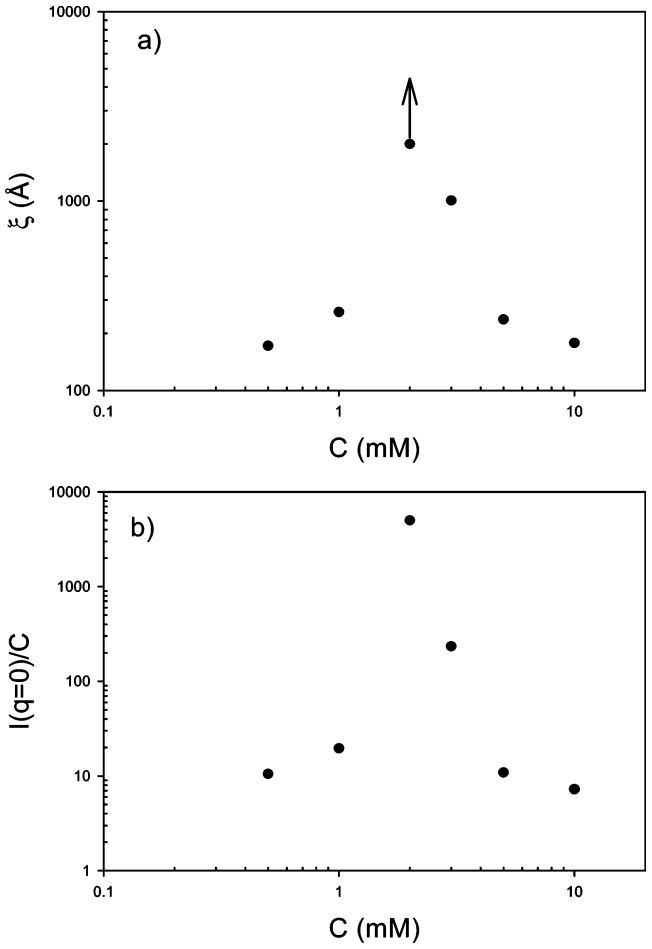


**Figure 9.** Concentration dependence of the (a) correlation length $\xi$ and of the (b) scattered intensity at zero-wave vector $I(q=0)$ at $T = 25$ °C.

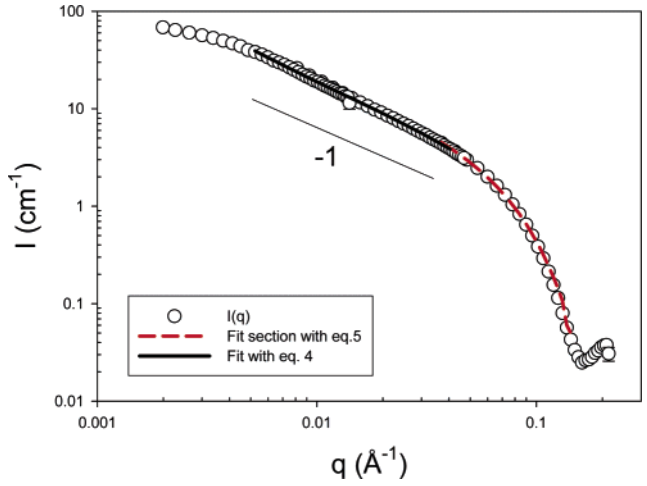


**Figure 10.** SANS spectra obtained for a 10 mM solution of $[AA9:BB]_n$ at 25 °C in decane. The black line represents the fit of the data in the intermediate regime with eq 4, and the dashed line represents the fit of the high $q$ data by a Guinier expression for the form factor of the section (eq 5).

form factor of the section

$$V_{\text{chain}}P(q) = \frac{\pi S}{q}\exp\left(\frac{-q^2 r_c^{\,2}}{2}\right) \tag{5}$$

where $r_c$ is the radius of gyration of the cross section. From these fits one can determine the mass per unit length $M_l$ of the fibrillar agregates, the section $S$, and the radius of gyration $r_c$ of the cross section. From the fits of Figure 10 we obtain $M_l = 515$ g mol$^{-1}$ Å$^{-1}$, $S = 1027$ Å$^2$, and $r_c = 17.6$ Å.

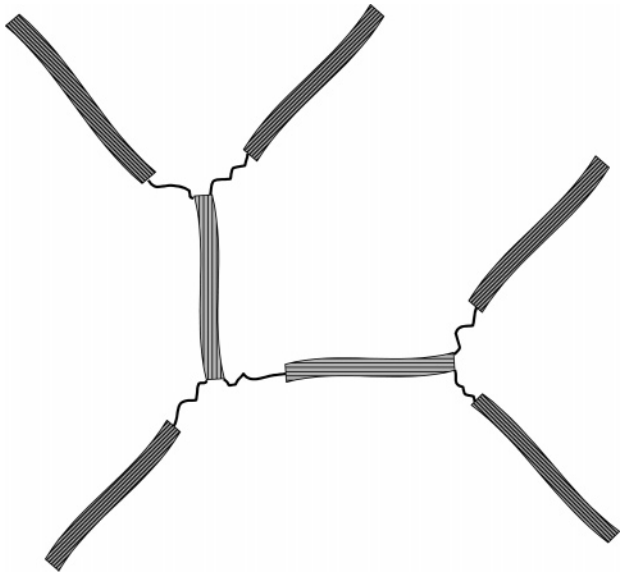

**Figure 11.** Microgel-like aggregate in the vicinity of $C^*$.

It must be noted that the fit using expressions 4 and 5 improves as the concentration increases, the $q^{-1}$ behavior being obtained in the semidilute regime, whereas the exponent of the power law for $C \ll C^*$ is slightly larger than 1, up to 1.3 for the most dilute sample. At the same time, the dip observed in the high $q$ range becomes more pronounced as the concentration increases. These two effects might be associated with a polydispersity in the section of the fibrillar aggregates which would be reduced at high concentration.

Turning now to the behavior in the vicinity of $C^*$, the scattering curve for the sample at $C = 2$ mM (Figure 7) could be fitted satisfactorily with the form factor of a wormlike Gaussian chain model with a persistance length of the order of 20 nm. This structure is rather unlikely, considering the quite large section and mass per unit length which should confer a rather high rigidity to the polymeric aggregates.

An alternative is provided by the formation of a microgel-like aggregate (Figure 11) where the short rods would be connected together when approaching the overlap concentration.

The crossover volume fraction, $\phi^*$, for a dispersion of long rods was found to be[27]

$$\phi^* = \frac{30S}{L^2} \tag{6}$$

Using this expression and the experimental values of $S$ and $\phi^*$ (0.6%), one obtains $L = 227$ nm, in reasonable agreement with the value that can be interpolated from the graph of Figure 9a discarding the upturn in the vicinity of $C^*$ ($\xi = 400$ Å, $L = 240$ nm).

**Molecular Packing.** To interpret the values obtained for $M_l$, $S$, and $r_c$, some speculations on the molecular packing can be made. If the fibrillar species consist of straight monomolecular wires, then the mass per unit length can be calculated to be about 48 g mol$^{-1}$Å$^{-1}$, a much lower value than the experimental determination 515 g mol$^{-1}$Å$^{-1}$. To explain such a difference, one could invoke a stacking of the disk-shaped aromatic rings of the molecules involving a folding of the monomolecular chains, as observed in ressembling systems forming columnar mesophases.[3a] In the latter case, the columnar superstructure

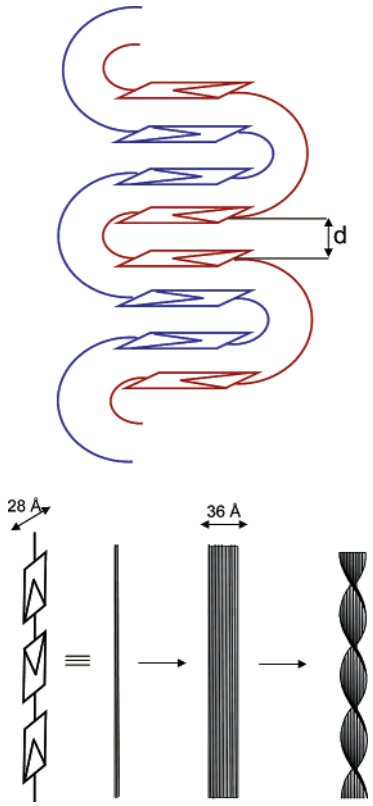


**Figure 12.** Possible structures of the fibrillar aggregates formed by the $[AA9:BB]_n$ supramolecular polymer. (a) Molecular folding with interpenetration of two chains; $d = 3.4$ Å. (b) Intermolecular stacking of straight monomolecular chains. The lateral aliphatic chains have not been represented.

was found to be formed by three polymeric strands having a triple helix conformation. In the present case, one could envision a folding and an interpenetration of two monomolecular chains, according to the schema of Figure 12a. Such a superstructure would account for the different lengths of the two spacers between the aromatic rings, but it is not favored by the presence of long lateral aliphatic chains. Furthermore, the calculation of the mass per unit length based on such a model would lead to a value of 318 g $mol^{-1}$ $Å^{-1}$, still significantly lower than the experimental value 515 g $mol^{-1}$ $Å^{-1}$. However, some limited additional aggregation of the chains is possible so that the average number of monomolecular chains within a fibril would be about 1.6, if one takes $d = 3.4$ Å as the inter-ring stacking distance.

Another possible model is based on an intermolecular stacking linking the linear molecular wires to form possibly helicoidal ribbons as represented in Figure 12b. Under this assumption, aggregates with an average degree of aggregation of 10.7 individual chains would account for the value of $M_l$. It can be assumed that the number of chains within a fibrillar aggregate would be limited by the torsion of the ribbon induced by the intrinsic chirality of the molecule.

Taking 3.4 Å as the intermolecular distance resulting from the stacking and using the experimental value of the cross section 1027 $Å^2$, the ribbon side lengths would be $a = 36$ Å and $b = 28.5$ Å. The latter value is in good agreement with molecular parameters. The radius of gyration of the cross section of such a ribbon is given by

$$r_c^2 = \frac{1}{12}(a^2 + b^2) \qquad (7)$$

Using the experimental values of $a$ and $b$, one obtains $r_c = 13.3$ Å, which is a value somewhat smaller than the experimental value 17.6 Å. The difference might be due to polydispersity of the fibril section, as the $r_c$ measured is a $z$ average, whereas the aggregation number deduced from $M_l$ is a number average. It must be reminded that electron microscopy experiments performed on dispersions of the same monomers in toluene have shown the presence of helical fibers similar to those presented in Figure 12b but with a much thicker cross section than the one measured in this study by SANS.[10]

Also, one can note that multichain ribbons would easily make interconnections in the vicinity of $C^*$ to form microgel aggregates such as those represented schematically in Figure 11.

## 5. Conclusion

Dispersions of the two homoditopic heterocomplementary monomers AA9 and BB in decane lead to the formation of supramolecular polymeric entities $[AA9:BB]_n$, giving gellike systems at very low concentration. This is due to the self-organization of the supramolecular polymer into long rigid fibers with well-defined given values of the cross section and the mass per unit length, in the concentration and temperature ranges investigated, as shown by the results of the SANS investigations. Studies in the dilute regime indicate that the average length increases with concentration, in agreement with the theoretical predictions for equilibrium polymers. In the semidilute regime, the correlation length is found to decrease upon increasing concentration as in a solution of an interpenetrating classical polymer. In the vicinity of the crossover concentration $C^*$, an unexpected increase of the aggregate size is observed, suggesting a percolation phenomenon. From the values of the cross section and the mass per unit length of the fibers, it can be inferred that a stacking of the aromatic rings occurs, either according to an intramolecular folding or a lateral aggregation of a dozen of unfolded monomolecular wires. No unambiguous proof in favor of either one of these structures can be given, but in any case each fiber contains on the average more than one supramolecular wire, with some indication of a nonnegligible polydispersity of the section.

The results obtained in this study indicate that the structural and consequently rheological properties of the $[AA9:BB]_n$ supramolecular polymeric systems are controlled by three main factors: the heterocomplementary of the molecular monomers, the strengthening of the hydrogen bonding through the choice of an appropriate solvent with a very low solubility of both monomers, and finally the stacking of the aromatic rings contained in the supramolecular chains.

**Acknowledgment.** The authors gratefully acknowledge V. Berl for his advice on the synthetic procedures and R. Schweins for his help during the SANS experiments.

## References and Notes

(1) (a) Ciferri, A. *Supramolecular Polymers;* Dekker: New York, 2000. (b) Brunsveld, L.; Folmer, B. J. B.; Meijer, E. W.; Sijbesma, R. P. *Chem. Rev.* **2001**, *101*, 4071. (c) Lehn, J. M. *Polym. Int.* **2002**, *51*, 825. (d) Moore, J. S. *Curr. Opin. Colloid Interface Sci.* **1999**, *4*, 108. (e) Paleos, C. M.; Tsiourvas, D. *Adv. Mater.* **1997**, *9*, 695. (f) Sherrington, D. C.; Taskinen, K. A. *Chem. Soc. Rev.* **2001**, *30*, 83. (g) Schmuck, C.; Wienand, W. *Angew. Chem., Int. Ed.* **2001**, *40*, 4363.

(2) *Procl. Natl. Acad. Si. U.S.A.* (Special Edition on Self-Assembly Processes) **2002**, *99*, 8.

(3) (a) Fouquey, C.; Lehn, J. M.; Levelut, A. M. *Adv. Mater.* **1990**, *2*, 254. (b) Prins, L. J.; Reinhoudt, D. N.; Timmerman, P. *Angew. Chem.* **2001**, *113*, 2446. (c) Hirschberg, K.; Brunsveld, J.; Ramzi, A.; Vekemans, J. A. J.; Sijbesma, R. P.; Meijer, E. W. *Nature (London)* **2000**, *38*, 2870. (d) Ikkala, O.; ten Brinke, G. *Science* **2002**, *295*, 2407.

(4) Bergbreiter, D. E. *Angew. Chem., Int. Ed. Engl.* **1980**, *19*, 2870.
(5) Schubert, U. S.; Eschbaumer, C. *Angew. Chem., Int. Ed.* **2002**, *41*, 2892.
(6) Meyer, E.; Castellano, R. K.; Diederich, F. *Angew. Chem., Int. Ed.* **2003**, *42*, 1210.
(7) Lasic, D. D.; Papahadjopoulos, D. *Science* **1995**, *267*, 1275.
(8) (a) Kotera, M.; Lehn, J. M.; Vigneron, J. P. *J. Chem. Soc., Chem. Commun.* **1994**, *197*. (b) Kotera, M.; Lehn, J. M.; Vigneron, J. P. *Tetrahedron* **1995**, *51*, 1953.
(9) (a) Lehn, J. M.; Mascal, M.; DeCian, A.; Fischer, J. *J. Chem. Soc., Chem. Commun.* **1990**, *479*. (b) Lehn, J. M.; Mascal, M.; DeCian, A.; Fischer, J. *J. Chem. Soc., Perkin Trans.* **1992**, *461*.
(10) Berl, V.; Schmutz, M.; Krische, M. J.; Khoury, R. G.; Lehn, J. M. *Chem.—Eur. J.* **2002**, *8*, 1227.
(11) Ikeda, M.; Nobori, T.; Schmutz, M.; Lehn, J. M. *Chem.—Eur. J.* **2005**, *11*, 662.
(12) (a) Sijbesma, R. P.; Beijer, F. H.; Brunsveld, L.; Folmer, B. J. B.; Hirschberg, J. H. K.; Lange, R. F. M.; Lowe, J. K. L.; Meijer, E. W. *Science* **1997**, *278*, 1601. (b) Folmer, B. J. B.; Cavini, E.; Sijbesma, R. P.; Meijer, E. W. *Chem. Commun.* **1998**, *1847*.
(13) Lillya, C. P.; Baker, R. J.; Hütte, S.; Winter, H. H.; Lin, Y. G.; Shi, J.; Dickinson, C.; Chien, J. C. W. *Macromolecules* **1992**, *25*, 2076.
(14) (a) Lee, C. M.; Jariwala, C. P.; Griffin, A. C. *Polymer* **1994**, *35*, 4550. (b) Bladon, P.; Griffin, A. C. *Macromolecules* **1993**, *26*, 6604. (c) Alexander, C.; Jariwala, C. P.; Lee, C. M.; Griffin, A. C. *Macromol. Chem., Macromol. Symp.* **1994**, *77*, 283. (d) St. Pourcain, C. B.; Griffin, A. C. *Macromolecules* **1995**, *28*, 4116.
(15) Choi, I. S.; Li, X.; Simanek, E. E.; Akaba, R.; Whitesides, G. M. *Chem. Mater.* **1999**, *11*, 684.
(16) (a) Abed, S.; Boileau, S.; Bouteiller, L.; Lacoudre, N. *Polym. Bull. (Berlin)* **1997**, *39*, 317. (b) He, C.; Lee, C. M.; Griffin, A. C.; Bouteiller, L.; Lacoudre, N.; Boileau, S.; Fouquet, C.; Lehn, J. M. *Mol. Cryst. Liq. Cryst.* **1999**, *332*, 251. (c) Lortie, F.; Boileau, S.; Bouteiller, L.; Chassenieux, C.; Demé, B.; Ducouret, G.; Jalabert, M.; Laupretre, F.; Terech, P. *Langmuir* **2002**, *18*, 7218.
(17) Kato, T.; Fujumasa, M.; Fréchet, J. M. J. *Chem. Mater.* **1995**, *7*, 368.
(18) Kihara, H.; Fréchet, J. M. J. *Liq. Cryst.* **1998**, *24*, 413.
(19) Kihara, H.; Kato, T.; Uryu, T.; Fréchet, J. M. J. *Chem. Mater.* **1996**, *8*, 961.
(20) Kato, T.; Kihara, H.; Kumar, U.; Uryu, T.; Fréchet, J. M. J. *Angew. Chem., Int. Ed. Engl.* **1994**, *33*, 1644.
(21) Kato, T.; Ihata, O.; Ujiie, S.; Tokita, M.; Watanabe, J. *Macromolecules* **1998**, *31*, 3551.
(22) Kato, T.; Kubota, Y.; Nakano, M.; Uryu, T. *Chem. Lett.* **1995**, *1127*.
(23) Castellano, R. K.; Rudkevich, D. M.; Rebek, J., Jr. *Proc. Natl. Acad. Sci. U.S.A.* **1997**, *94*, 7132.
(24) Seto, C. T.; Whitesides, G. M. *J. Am. Chem. Soc.* **1993**, *115*, 905.
(25) Kolomiets, E.; Lehn, J. M., unpublished results.
(26) des Cloizeaux, J. *Macromolecules* **1973**, *6*, 403.
(27) Mori, Y.; Ookubo, N.; Hayakawa, R.; Wada, Y. *J. Polym. Sci.* **1982**, *20*, 2111.

MA0523522